AAPS PharmSciTech, Vol. 14, No. 1, March 2013 (© 2013)
DOI: 10.1208/s12249-012-9917-x

Research Article

Angular Circulation Speed of Tablets in a Vibratory Tablet Coating Pan

Rahul Kumar[1] and Carl Wassgren[1,2,3]

Received 10 October 2012; accepted 14 December 2012; published online 17 January 2013

Abstract. In this work, a single tablet model and a discrete element method (DEM) computer simulation are developed to obtain the angular circulation speed of tablets in a vibratory tablet coating pan for range of vibration frequencies and amplitudes. The models identify three important dimensionless parameters that influence the speed of the tablets: the dimensionless amplitude ratio (a/R), the Froude number ($a\omega^2/g$), and the tablet–wall friction coefficient, where a is the peak vibration amplitude at the drum center, ω is the vibration angular frequency, R is the drum radius, and g is the acceleration due to gravity. The models predict that the angular circulation speed of tablets increases with an increase in each of these parameters. The rate of increase in the angular circulation speed is observed to decrease for larger values of a/R. The angular circulation speed reaches an asymptote beyond a tablet–wall friction coefficient value of about 0.4. Furthermore, it is found that the Froude number should be greater than one for the tablets to start circulating. The angular circulation speed increases as Froude number increases but then does not change significantly at larger values of the Froude number. Period doubling, where the motion of the bed is repeated every two cycles, occurs at a Froude number larger than five. The single tablet model, although much simpler than the DEM model, is able to predict the maximum circulation speed (the limiting case for a large value of tablet–wall friction coefficient) as well as the transition to period doubling.

KEY WORDS: coating; discrete element method; granular materials; pharmaceuticals; vibration.

INTRODUCTION

There has been a recent move towards continuous coating in the pharmaceutical industry to take advantage of the improved productivity and robustness of continuous processes (1). The diameter of a continuous coater drum is much smaller compared with production batch coaters, for which the drum diameter can be as large as 1.5 m. Due to the small bed depth, tablets appear more frequently in the spray region of a continuous coater, thus leading to better coating uniformity and achieving the target coating mass in less time compared with batch coating. Shorter coating times also amount to energy savings (electricity, energy required for compression, and heating of drying air). Marjeram (2) estimated that moving from batch to continuous coating can reduce the cost, per kilogram of tablets coated, by about a factor of five.

Continuous coating also provides better control and monitoring of the coating process. Due to the continuous discharge, coated tablets are available for inspection and testing within a short period of time after the coating process is started. Any issues with the coating quality can be identified at this point and corrected, affecting only a relatively small number of tablets.

Despite the advantages that continuous coaters offer, there are some limitations as well. For example, continuous tablet coaters are generally designed for high volume products, such as neutraceuticals. For small throughputs, *e.g.*, less than 100 kg/h, the size of the drum for a continuous coater needs to be reduced to maintain a deep enough bed to cause the tablet bed to circulate and mix. There is, however, a lower limit on the diameter of the drum, which is dictated by the need to fit the spray nozzles. If the drum is too small, the spray-to-bed distance will be small, leading to a smaller spray area which may cause over-wetting of the tablets. Furthermore, if the spray is too close to the bed, the dynamic pressure of the atomizing air creates a large depression in the bed, adversely affecting the tablet motion and coating uniformity.

To overcome these problems, a new vibratory mechanism has been proposed to produce circulatory motion of the tablet bed and is currently in a prototype stage at O'Hara Technologies (Richmond Hill, Ontario, Canada). A schematic of the vibratory coater is shown in Fig. 1. An immediate advantage of not having a rotating drum is that the drum can be open at the top, thus allowing the spray to be placed at an optimal location. Additionally, the open design enables easy access for in-line sensors to monitor the coating process.

The angular circulation speed of tablets, *i.e.*, rate at which the angular position of the tablets changes about the center of the drum, is an important parameter which affects inter-tablet coating variability, defined as the ratio of the standard deviation to the mean of the total coating mass distribution over all the tablets. Several modeling approaches have been used to

[1] School of Mechanical Engineering, Purdue University, West Lafayette, Indiana 47907, USA.
[2] Department of Industrial and Physical Pharmacy, Purdue University, West Lafayette, Indiana 47907, USA.
[3] To whom correspondence should be addressed. (e-mail: wassgren@purdue.edu)

 1530-9932/13/0100-0339/0 © 2013 American Association of Pharmaceutical Scientists

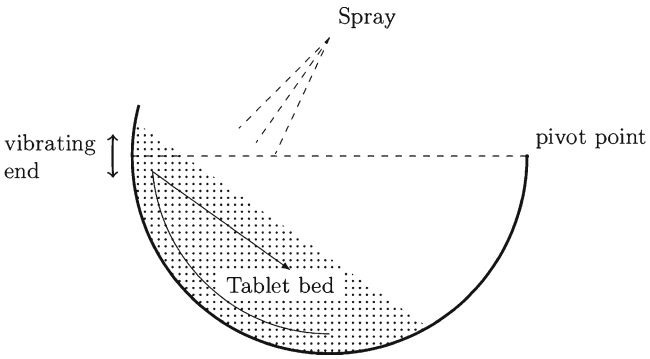

Fig. 1. Schematic of the vibratory coater

predict inter-tablet coating variability for a batch coating operation (3–7) and more recently for continuous coaters (8,9). Mann (4) obtained an expression for CoV_{inter} using renewal theory, in terms of the distributions of the time spent by the tablets in the spray zone per pass and the cycle time, given by,

$$CoV_{\text{inter}} = \sqrt{\left(\frac{\sigma_m}{\mu_m}\right)^2 \frac{\mu_C}{T_{\text{coat}}} + \left(\frac{\sigma_C}{\mu_C}\right)^2 \frac{\mu_C}{T_{\text{coat}}}}, \qquad (1)$$

where μ_m and σ_m denote the mean and standard deviation of the distribution of coating mass deposited on a tablet per pass, μ_C and σ_C denote the mean and standard deviation of the cycle time distribution, and T_{coat} is the total coating time. Furthermore, since the amount of coating that a tablet receives is nearly directly proportional to the total time it spends in the spray zone, Eq. 1 can be written as,

$$CoV_{\text{inter}} = \sqrt{\left(\frac{\sigma_T}{\mu_T}\right)^2 \frac{\mu_C}{T_{\text{coat}}} + \left(\frac{\sigma_C}{\mu_C}\right)^2 \frac{\mu_C}{T_{\text{coat}}}}, \qquad (2)$$

where μ_T and σ_T denote the mean and standard deviation of the distribution of the spray zone residence time per pass. Note that prior work in rotating drum coaters has shown that the cycle time is a strong function of the angular circulation speed, with the mean cycle time reducing as the angular circulation speed increases (10–12). The standard deviation in the mean cycle time has also been found to decrease as drum speed increases (11). The mean and standard deviation of the spray zone residence time has also been found to decrease at larger angular circulation speeds (11–13). Thus, the inter-tablet coating variability is expected to be smaller for larger angular circulation speeds.

Using vibration to produce circulatory motion of particulate material is not very common. Vibratory conveyors and feeders that produce translation motion are, however, quite commonly used for the transport of granular material, mainly in the mining and food industries. There is, thus, considerable published work on vibratory conveyors and feeders, which has focused on particle dynamics and the dependence of conveying speed and efficiency on the frequency and amplitude of vibrations.

The following assumptions are commonly made in developing theoretical models for vibratory conveyors (14–17):

1. The vibration is simple harmonic.
2. The bulk material can be treated as a point mass system located at its center of mass, acted on by frictional forces, gravity, and the vibrating trough.
3. Air resistance when the material is thrown into the air is negligible.

Ng *et al.* (14) developed a computer model for the motion of granular material on an inclined, vibrating trough. A further assumption that was made in this analysis is that the coefficient of restitution of the bulk material bed on the vibrating deck was assumed to be zero. Based on the acceleration of the material in directions normal and tangential to the trough, three different modes of motion were identified: a stationary phase in which the bed rests on the trough, a sliding phase in which the bed slides along the trough, and a flight or throw phase in which the bed is thrown in the air. A model was used to calculate the acceleration of the bed and manage the transition between the phases. Good agreement was found between the model predictions and experiments, supporting the point mass system assumption.

Rademacher and ter Borg (17) presented a detailed mathematical analysis in which they formally introduced the throw number, a dimensionless number that governs if the particles go into the flight phase, and the transport velocity, which is the average conveying velocity of particles during a full period. A detailed analysis for the collision phase was also presented in which the increase in friction force due to the impulsive normal force during the contact was taken into account to compute the change in tangential velocity during the collision.

Lim (16) studied the effect of friction coefficient on the conveying speed for an inclined vibrating conveyor and found that the conveying speed increases as the friction coefficient is increased, up to a friction coefficient of about 0.7. The model predictions of mean conveying speed were also in good agreement with experimentally measured values.

While these models have been shown to give good agreement with experimental data, an important difference between vibratory conveyors and a vibratory coater is that vibratory conveyors are designed to produce translational motion of the material bed while the vibratory coater is designed for circulatory motion within the material (tablet) bed without translational motion of the bulk. This difference in the type of motion produced has a strong implication on the assumption of treating the bulk material as a point mass. Clearly, if the bed is assumed to be a point mass, circulatory motion within the bed cannot be studied. Thus, for the vibratory coater, the motion of individual particles in the bed needs to be considered.

The discrete element method (DEM) has also been used to examine the motion of granular material due to vibrations. DEM solves for the motion of individual particles in the system based on the forces acting on them, such as gravity and other contact forces. Typical outputs from DEM include the position, orientation, and velocity (both translational and angular) of all the particles in the system as well as the forces and torques acting at the particle–particle and particle–boundary contacts at all instants in time.

Wassgren *et al.* (18) studied the motion of a deep bed of granular material undergoing vertical vibrations in a rectangular container. Several phenomena such as heaping, surface waves, and arching were observed depending on the vibration frequency and amplitude. They found that the important dimensionless parameters that influence the state of the particle bed are h_0/d,$a\omega^2/g$, and a/d, where a is the vibration peak amplitude, ω is the radian frequency of vibration, d is the

particle diameter, h_0 is the initial particle bed depth, and g is the acceleration due to gravity. A period-doubling bifurcation of the motion was also reported, where instead of repeating the same motion every oscillation cycle, the motion of the bed is repeated every two cycles. This bifurcation can lead to sections of the particle bed oscillating out of phase, producing an arching behavior.

Using experiments and DEM simulations, Naeini (19) studied the 2-D motion of spheres in a tub-finisher (used for cleaning, polishing, and deburring of mechanical parts) undergoing inclined vibrations. The circulation of the spheres was found to increase with the depth of particulate media and with the magnitude of the particle–wall and particle–particle friction coefficients. The strength of circulation was also found to increase with the vibration amplitude. DEM predictions were consistently smaller than experiments, which was attributed to a lack of a rolling resistance model in the DEM simulations.

The focus of this work is to investigate the influence of vibration frequency and amplitude, and the tablet–wall friction coefficient on the angular circulation speed of tablets in a vibratory coater. A single tablet model and a more complex and time consuming DEM model are developed to study the effect of these parameters on the angular circulation speed.

MATERIALS AND METHODS

Single Tablet Model

The single tablet model uses Newton's laws of motion to solve for the trajectory of a single tablet due to the vibration of the drum. The effects of atomizing and drying air on the motion of the tablets have been neglected. Since the motion of only a single tablet is considered, the computational time is much smaller (~seconds) compared with the more complex and time consuming DEM simulations (~hours to a few days). Although the model developed in this section is greatly simplified, it provides helpful information on the parameters affecting tablet circulatory speed and the speed's functional dependence on these parameters.

Figure 2 shows a schematic of the system under consideration. The system consists of an oscillating two-dimensional cylindrical pan. The local xy-coordinate system has the x-axis along the pan diameter, which passes through the pivot point, P, and oscillates with the drum. The global $x_G y_G$-coordinate system is fixed, with the x_G axis along the initial horizontal position of the pan diameter.

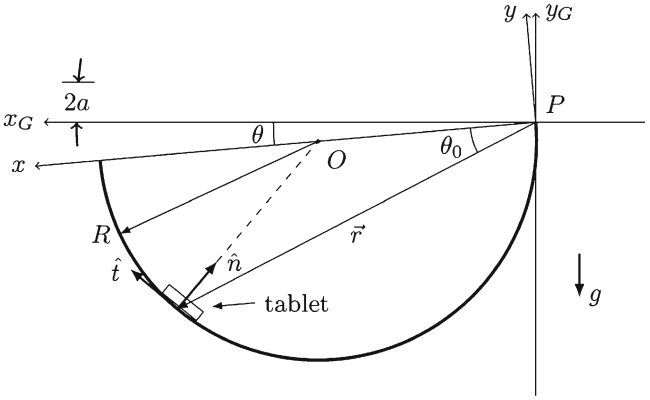

Fig. 2. Single tablet model for the vibratory coater

Consider a single tablet contained within this pan. The tablet's acceleration in this local, rotating frame of reference is,

$$\vec{a}_r = \vec{a}_i - 2\vec{\Omega} \times \vec{v}_r - \vec{\Omega} \times \left(\vec{\Omega} \times \vec{r}\right) - \frac{\mathrm{d}\vec{\Omega}}{\mathrm{dt}} \times \vec{r}, \qquad (3)$$

where $\vec{a}_r = \left(\frac{\mathrm{d}^2\vec{r}}{\mathrm{dt}^2}\right)_r$ is the apparent acceleration in the rotating reference frame, $\vec{a}_i$ is the acceleration in the absolute frame of reference, $\vec{\Omega}$ is the angular velocity of the rotating frame, $\vec{r}$ is the position vector of the tablet, and $\vec{v}_r$ is the tablet velocity in the rotating frame of reference. The term $-\vec{\Omega} \times \left(\vec{\Omega} \times \vec{r}\right)$ represents the centripetal acceleration and the term $-2\vec{\Omega} \times \vec{v}_r$ is the Coriolis acceleration.

Since the frame is oscillating about the z-axis, the angular position of the initially horizontal diameter, θ, due to the vibration is,

$$\theta = \theta_{\max} \sin(\omega t) \qquad (4)$$

where $\theta_{\max}$ is the maximum angle of vibration (=a/R), a is the vibration amplitude at the center of the drum, R is the drum radius, and ω is the vibration angular frequency. Thus, the angular velocity of the reference frame is,

$$\vec{\Omega} = \Omega\hat{k} = \dot{\theta}\hat{k} = (a\omega/R)\cos(\omega t)\hat{k}, \qquad (5)$$

where $\hat{k}$ is the unit vector in the z direction. The angular acceleration of the reference frame is,

$$\frac{\mathrm{d}\vec{\Omega}}{\mathrm{dt}} = \ddot{\theta}\hat{k} = -\left(a\omega^2/R\right)\sin(\omega t)\hat{k}. \qquad (6)$$

Since the only non-zero component of $\vec{\Omega}$ is in the z direction, the centripetal acceleration term reduces to,

$$-\vec{\Omega} \times \left(\vec{\Omega} \times \vec{r}\right) = \Omega^2\vec{r}. \qquad (7)$$

Consider the tablet as shown in Fig. 2. The position vector of the tablet, $\vec{r}$, in the rotating frame of reference is,

$$\vec{r} = (2R\cos\theta_0)\left[\cos(\theta_0)\hat{i} - \sin(\theta_0)\hat{j}\right], \qquad (8)$$

where θ_0 is the angle the position vector makes with the line passing through the drum center and the pivot point, and $\hat{i}$ and $\hat{j}$ are the unit vectors in the x and y directions, respectively.

Similar to the work by Rademacher and ter Borg (17), three phases of motion can be identified:

- Rest phase—the tablet is at rest relative to the drum surface.
- Sliding phase—the tablet is sliding on the drum surface.
- Flight phase—the tablet loses contact with the drum surface and follows a ballistic trajectory before hitting the drum surface.

Rest Phase

In the rest phase, the velocity and acceleration of the tablet in the rotating frame of reference is zero, *i.e.*, $\vec{v}_r = 0$

and $\vec{a}_r = 0$. Using Eq. 3, the acceleration of the tablet in the rotating frame of reference simplifies to,

$$\vec{0} = \vec{a}_i + \Omega^2 \vec{r} - \frac{\mathrm{d}\vec{\Omega}}{\mathrm{dt}} \times \vec{r}. \tag{9}$$

Depending on the forces in the normal and tangential direction, the tablet may transition to a sliding phase or directly to the flight phase. Each of these cases is considered in the following sub-sections.

Transition to Sliding Phase

If the sum of the tangential force acting on the tablet due to gravity, the centrifugal force, and the Coriolis force exceeds the maximum Coulomb friction force, then the tablet slides on the drum surface. The transition from the rest phase to a sliding phase can thus be examined by looking at the force balance in the tangential direction. Taking the dot product of Eq. 9 with the tangent vector, $\hat{t} = \sin(2\theta_0)\hat{i} + \cos(2\theta_0)\hat{j}$, gives,

$$0 = \vec{a}_i.\hat{t} + \Omega^2 \vec{r}.\hat{t} - \left(\frac{\mathrm{d}\vec{\Omega}}{\mathrm{dt}} \times \vec{r}\right).\hat{t}. \tag{10}$$

The first term on the right hand side, $\vec{a}_i.\hat{t}$ is the component of the acceleration in the inertial frame in the direction of the tangent vector, and is equal to the sum of the forces in the tangent direction divided by the mass. The forces acting in the tangent direction are the friction force and weight. The first term can be written as,

$$\vec{a}_i.\hat{t} = \pm f/m - g\cos(2\theta_0 + \theta), \tag{11}$$

where the direction of the friction force, f, is opposite to the direction of the tangential velocity relative to the drum.

The second term in Eq. 10 can be written as,

$$\begin{aligned} \Omega^2 \vec{r}.\hat{t} &= 2\Omega^2 R\cos\theta_0(\cos\theta_0\sin 2\theta_0 - \sin\theta_0\cos 2\theta_0 \\ &= 2\Omega^2 R\cos\theta_0\sin\theta_0 \\ &= 2\tfrac{a^2\omega^2}{R}\cos^2(\omega t)\cos\theta_0\sin\theta_0, \end{aligned} \tag{12}$$

where the trigonometric identity,

$$\sin\alpha\cos\beta - \cos\alpha\sin\beta = \sin(\alpha - \beta), \tag{13}$$

has been used. To evaluate the last term, note that,

$$\frac{\mathrm{d}\vec{\Omega}}{\mathrm{dt}} \times \vec{r} = 2R\cos\theta_0 \frac{\mathrm{d}\Omega}{\mathrm{dt}}\left(\sin\theta_0\hat{i} + \cos\theta_0\hat{j}\right). \tag{14}$$

Taking the dot product with the tangent vector gives,

$$\begin{aligned} \left(\tfrac{\mathrm{d}\vec{\Omega}}{\mathrm{dt}} \times \vec{r}\right).\hat{t} &= 2R\cos\theta_0 \tfrac{\mathrm{d}\Omega}{\mathrm{dt}}(\sin\theta_0\sin 2\theta_0 + \cos\theta_0\cos 2\theta_0) \\ &= 2R\cos^2\theta_0 \tfrac{\mathrm{d}\Omega}{\mathrm{dt}} \\ &= -2a\omega^2\cos^2\theta_0\sin(\omega t), \end{aligned}$$

where the trigonometric identity, (15)

$$\cos\alpha\cos\beta + \sin\alpha\sin\beta = \cos(\alpha - \beta), \tag{16}$$

has been used. Collecting all terms together, Eq. 10 can be written as,

$$\begin{aligned} 0 = \pm f/m - g\cos(2\theta_0 + \theta) + 2\frac{a^2\omega^2}{R}\cos^2(\omega t) \\ \times \cos\theta_0\sin\theta_0 + 2a\omega^2\cos^2\theta_0\sin(\omega t), \end{aligned} \tag{17}$$

which can be re-arranged to give,

$$\begin{aligned} \pm f/m = g\cos(2\theta_0 + \theta) - 2\frac{a^2\omega^2}{R}\cos^2(\omega t)\cos\theta_0\sin\theta_0 \\ - 2a\omega^2\cos^2\theta_0\sin(\omega t). \end{aligned} \tag{18}$$

For the tablet to slide on the drum surface, the magnitude of the friction force should exceed the upper limit of μN specified by Coulomb friction, *i.e.*,

$$\left| g\cos(2\theta_0 + \theta) - 2\frac{a^2\omega^2}{R}\cos^2(\omega t)\cos\theta_0\sin\theta_0 - 2a\omega^2\cos^2\theta_0\sin(\omega t) \right| \geq \mu N/m. \tag{19}$$

The normal force, N, required in Eq. 19 can be computed by considering the force balance in the normal direction. Taking the dot product of Eq. 9 with the normal vector, $\hat{n} = -\cos(2\theta_0)\hat{i} + \sin(2\theta_0)\hat{j}$, gives,

$$0 = \vec{a}_i.\hat{n} + \Omega^2 \vec{r}.\hat{n} - \left(\frac{\mathrm{d}\vec{\Omega}}{\mathrm{dt}} \times \vec{r}\right).\hat{n}. \tag{20}$$

The first term, $\vec{a}_i.\hat{n}$, is the component of the acceleration in the inertial frame in the direction of the normal vector and is equal to the sum of the forces in the normal direction divided by the mass. The forces acting in the normal direction are the normal force and weight. The first term can thus be written as,

$$\vec{a}_i.\hat{n} = N/m - g\sin(2\theta_0 + \theta). \tag{21}$$

The second term can be written as,

$$\begin{aligned} \Omega^2 \vec{r}.\hat{n} &= -2\Omega^2 R\cos\theta_0(\cos\theta_0\cos 2\theta_0 + \sin\theta_0\sin 2\theta_0) \\ &= -2\Omega^2 R\cos^2\theta_0 \\ &= -2\tfrac{a^2\omega^2}{R}\cos^2(\omega t)\cos^2\theta_0, \end{aligned} \tag{22}$$

where the trigonometric identity given in Eq. 16 has been used. Evaluating the last term gives,

$$\begin{aligned} \left(\tfrac{\mathrm{d}\vec{\Omega}}{\mathrm{dt}} \times \vec{r}\right).\hat{n} &= 2R\cos\theta_0 \tfrac{\mathrm{d}\Omega}{\mathrm{dt}}(-\sin\theta_0\cos 2\theta_0 + \cos\theta_0\sin 2\theta_0) \\ &= 2R\cos\theta_0 \tfrac{\mathrm{d}\Omega}{\mathrm{dt}}\sin\theta_0 \\ &= -2a\omega^2\cos\theta_0\sin\theta_0\sin(\omega t), \end{aligned} \tag{23}$$

where the trigonometric identity given in Eq. 13 has been used. Collecting all terms together, Eq. 20 can be written as,

$$0 = N/m - g\sin(2\theta_0+\theta) - 2\frac{a^2\omega^2}{R}\cos^2(\omega t)\cos^2\theta_0 + 2a\omega^2\cos\theta_0\sin\theta_0\sin(\omega t), \tag{24}$$

which can be re-arranged to give,

$$N/m = g\sin(2\theta_0+\theta) + 2\frac{a^2\omega^2}{R}\cos^2(\omega t)\cos^2\theta_0 - 2a\omega^2\cos\theta_0\sin\theta_0\sin(\omega t). \tag{25}$$

Equation 25 along with Eq. 19 provides the necessary conditions for transition from the rest phase to the sliding phase.

Transition to Flight Phase

It is also possible for the tablet to go directly from the rest phase to the flight phase if the friction coefficient is large enough so that the condition in Eq. 19 is never met. In this case, the tablet will leave the surface when the normal force given in Eq. 25 becomes negative, which leads to the condition,

$$g\sin(2\theta_0+\theta) + 2\frac{a^2\omega^2}{R}\cos^2(\omega t)\cos^2\theta_0 - 2a\omega^2\cos\theta_0\sin\theta_0\sin(\omega t) < 0. \tag{26}$$

Dividing throughout by g and defining the Froude number, Fr,

$$Fr = a\omega^2/g, \tag{27}$$

gives,

$$\sin(2\theta_0+\theta) + 2\frac{a}{R}Fr\cos^2(\omega t)\cos^2\theta_0 - 2Fr\cos\theta_0\sin\theta_0\sin(\omega t) < 0. \tag{28}$$

Equation 28 implies that the phase angle at which a tablet leaves the drum surface is dependent on θ_0, a/R, and the Froude number. Furthermore, the dependence on a/R is weak since the amplitude is generally an order of magnitude smaller than the drum radius and thus the second term can generally be neglected. Additionally, using the fact that θ is generally much smaller than θ_0, a useful approximation to Eq. 28 can be written as,

$$\begin{aligned}\sin(2\theta_0) - 2Fr\cos\theta_0\sin\theta_0\sin(\omega t) &< 0\\ 1 - Fr\sin(\omega t) &< 0\\ \sin(\omega t) &> 1/Fr,\end{aligned} \tag{29}$$

which gives an approximate phase angle at which the tablet leaves the drum surface. Note the phase angle in Eq. 29 is independent of the location of the tablet on the drum surface (θ_0). The approximation amounts to neglecting the curvature of the drum surface, and thus the criterion given in Eq. 29 is the same as that obtained for vibrating conveyors (17).

Now examine the velocity of the tablet just after leaving the drum surface. The magnitude and direction of the velocity determines how far the tablet can "hop" while in flight. The speed of the tablet just after leaving the drum surface is,

$$\begin{aligned}\left|\vec{v}_{\text{takeoff}}\right| &= \left|\vec{\Omega}\times\vec{r}\right|\\ &= 2R\cos\theta_0\Omega\\ &= 2a\omega\cos(\omega t)\cos\theta_0,\end{aligned} \tag{30}$$

while the angle at which the tablet leaves the surface is θ_0 with respect to $\hat{t}$.

Sliding Phase

The equations of motion for the sliding phase are similar to those for the rest phase, except that the velocity and acceleration in the rotating frame of reference may now be non-zero. Taking the dot product of Eq. 3 with the tangent vector, $\hat{t} = \sin(2\theta_0)\hat{i} + \cos(2\theta_0)\hat{j}$, gives,

$$\vec{a}_r.\hat{t} = \vec{a}_i.\hat{t} - 2\vec{\Omega}\times\vec{v}_r.\hat{t} + \Omega^2\vec{r}.\hat{t} - \left(\frac{\mathrm{d}\vec{\Omega}}{\mathrm{dt}}\times\vec{r}\right).\hat{t}. \tag{31}$$

The additional term due to the Coriolis acceleration can be evaluated as follows,

$$\begin{aligned}2\left(\vec{\Omega}\times\vec{v}_r\right).\hat{t} &= 2\left(-\Omega v_{ry}\hat{i} + \Omega v_{rx}\hat{j}\right).\hat{t}\\ &= 2\left(\Omega v_{ry}\sin 2\theta_0 + \Omega v_{rx}\cos 2\theta_0\right),\end{aligned} \tag{32}$$

where v_{rx} and v_{ry} are the x and y components of the tablet velocity relative to the drum in the rotating frame of reference, respectively. Equation 31 can now be written as,

$$a_{rt} = \pm\mu N/m - g\cos(2\theta_0+\theta) - 2\left(\Omega v_{ry}\sin 2\theta_0 + \Omega v_{rx}\cos 2\theta_0\right) + 2\tfrac{a^2\omega^2}{R}\cos^2(\omega t)\cos\theta_0\sin\theta_0 + 2a\omega^2\cos^2\theta_0\sin(\omega t). \tag{33}$$

The normal force required in Eq. 33 is computed by considering the acceleration in the normal direction. Since the tablet is sliding along the drum surface, the acceleration in the normal direction in the drum frame of reference is zero. Taking the dot product of Eq. 3 with the normal vector, $\hat{n} = -\cos(2\theta_0)\hat{i} + \sin(2\theta_0)\hat{j}$, gives,

$$0 = \hat{a}_i.\hat{n} - 2\vec{\Omega}\times\vec{v}_r.\hat{n} + \Omega^2\vec{r}.\hat{n} - \left(\frac{d\vec{\Omega}}{dt}\times\vec{r}\right).\hat{n}. \tag{34}$$

All terms in Eq. 34, except for the Coriolis term, are the same as those used in the rest phase. The normal component of the Coriolis term can be computed as follows,

$$\begin{aligned}2\left(\vec{\Omega}\times\vec{v}_r\right).\hat{n} &= 2\left(-\Omega v_{ry}\hat{i} + \Omega v_{rx}\hat{j}\right).\hat{n}\\ &= 2\left(-\Omega v_{ry}\cos 2\theta_0 + \Omega v_{rx}\sin 2\theta_0\right).\end{aligned} \tag{35}$$

Substituting all of the terms into Eq. 34, gives,

$$0 = N/m - g\sin(2\theta_0+\theta) - 2\left(-\Omega v_{ry}\cos 2\theta_0 + \Omega v_{rx}\sin 2\theta_0\right) - 2\frac{a^2\omega^2}{R}\cos^2(\omega t)\cos^2\theta_0 + 2a\omega^2\cos\theta_0\sin\theta_0\sin(\omega t), \tag{36}$$

which can be re-arranged to obtain the expression for the normal force,

$$N/m = g\sin(2\theta_0+\theta) + 2\left(-\Omega v_{ry}\cos 2\theta_0 + \Omega v_{rx}\sin 2\theta_0\right) + 2\frac{a^2\omega^2}{R}\cos^2(\omega t)\cos^2\theta_0 - 2a\omega^2\cos\theta_0\sin\theta_0\sin(\omega t). \tag{37}$$

Equations 33 and 37 completely describe the motion of the tablet in the sliding phase.

Transition to Flight Phase

The tablet transitions to the flight phase when the normal force given by Eq. 37 equals zero. This event is similar to the condition for transitioning from the rest phase to the flight phase, except for the additional Coriolis force term. The speed at which the tablet leaves the drum surface is given by the magnitude of the sum of the drum velocity at the position of the tablet and the tablet's velocity in the rotating frame,

$$\left|\vec{v}_{\text{takeoff}}\right| = \left|\vec{\Omega}\times\vec{r} + \vec{v}_r\right|, \tag{38}$$

while the angle at which the tablet leaves the surface is θ_0 with respect to $\hat{t}$.

Transition to Rest Phase

The friction force acting in the direction opposite to the velocity of the tablet may decelerate the tablet to zero velocity, detected by a change in the sign of the velocity. At that instant, if Eq. 19 is satisfied, the tablet will start to slide in the opposite direction, otherwise it will transition to the rest phase.

Flight Phase

Once the speed and the angle at which the tablet leaves the drum surface are known, the trajectory of the tablet can be computed using the assumption of a ballistic trajectory. The projectile motion continues until the tablet hits the drum surface. Although the collision between a single tablet and the drum surface is not completely inelastic, the presence of other tablets in the system quickly dissipates all of the kinetic energy normal to the surfaces, making the collision nearly inelastic. Thus, it is further assumed that the collision with the drum surface is completely inelastic.

The equation of motion for the tablet in the flight phase is given by Eq. 3. The only force acting on the body during flight is due to the gravitation acceleration and, thus, $\vec{a}_i = \vec{g}$, resulting in,

$$\vec{a}_r = \vec{g} - 2\vec{\Omega}\times\vec{v}_r - \vec{\Omega}\times\left(\vec{\Omega}\times\vec{r}\right) - \frac{\mathrm{d}\vec{\Omega}}{\mathrm{dt}}\times\vec{r}. \tag{39}$$

The first three acceleration terms on the right hand side of Eq. 39 are the gravitational, Coriolis, and centripetal accelerations, respectively. The last term is due to the angular acceleration of the rotating frame.

Transition to Sliding Phase

While the tablet is in the flight phase, its distance from the center of the drum is calculated at the end of every time step and when that distance is equal to the drum radius, impact with the drum surface occurs. Note that since the check is performed only at the end of a time step, it is possible that the tablet goes slightly beyond the drum surface; however, this error is not very significant due to the small integration time step size used (1×10^{-4} s). When the tablet hits the drum surface, the component of the velocity normal to the drum is set to zero under the assumption of a fully inelastic collision. The tangential velocity is assumed not to change during the impact. Thus, the motion transitions to the sliding phase with the subsequent motion governed by the equations developed for the sliding phase.

Tablet Trajectory

The equations of motion in each of the phases and the conditions required to transition between phases are used to obtain the tablet's trajectory. An initial position of the tablet is specified on the drum surface and the equations of motion are integrated in time using a semi-implicit Euler time integration scheme. The tablet is initially at rest on the drum surface. A time step size of 1×10^{-4} s is used for the time integration. One of the cases was run using a smaller time step to ensure that the results are independent of the choice of time step size.

Discrete Element Model

The single tablet model can provide insight into the influence of various parameters that influence the motion of tablets in the pan. However, the effects of the simplifying assumptions of the single tablet motion on the predicted angular circulation speed of the tablets need to be investigated. For this purpose, a detailed DEM model is used to simulate the motion of tablets in the coating pan subjected to vibrations. A DEM model accounts for the contact forces between tablets and thus can be used to compare with the predictions from the single tablet model. In this work a soft-particle DEM algorithm is used.

Contact Detection

True biconvex tablets are used in the DEM simulations with the contact detection algorithms, referred to as fine contact detection, developed by Kodam *et al.* (20). The dimensions of the tablets are given in Table I and are close to the size of a typical 500 mg pharmaceutical tablet. Due to the computationally expensive nature of the contact detection algorithm, Kodam *et al.* (20) used an intermediate contact detection in which bounding spheres of the two tablets involved in the contact are checked for intersection as shown in Fig. 3. Clearly, if the bounding spheres do not intersect, the tablets cannot be in contact.

In this work, an enhanced intermediate contact detection algorithm is presented which can further reduce the number of

Table I. Characteristics of Tablets Used in the DEM Simulations

Band diameter (mm)	11.16
Band thickness (mm)	3.47
Cap thickness (mm)	1
Density (kg/m^3)	1,210

contacts to be checked by the fine contact detection algorithm. Consider again the scenario shown in Fig. 3. Even though the tablets are not in actual contact, the bounding spheres do intersect, and thus, the contact will be checked by fine contact detection, increasing the computational time.

In addition to the bounding sphere, two more spheres can be associated with any given tablet: one sphere associated with each cap of the tablet as shown in Fig. 4. For two tablets to be in actual contact, each of the three spheres associated with one tablet should be in contact with each of the three spheres associated with the other tablet. Thus, eight additional checks for sphere-sphere contact need to be performed. Even though additional sphere-sphere contacts need to checked, increasing the computational time for intermediate contact detection, these additional checks significantly reduce the number of contacts to be checked by the fine contact detection algorithm compared with just checking for bounding spheres. For example, the potential contact shown in Fig. 3 redrawn in Fig. 5 showing the cap spheres that do not intersect, will be filtered out.

Computationally, checking for sphere–sphere contacts takes a fraction of the time required to perform fine contact detection of biconvex tablets, thus, there is an overall reduction in computational time. Studies indicate that the enhanced intermediate contact detection reduces the number of contacts to be checked by fine contact detection to about one third, thus achieving about a threefold speedup in the contact detection step.

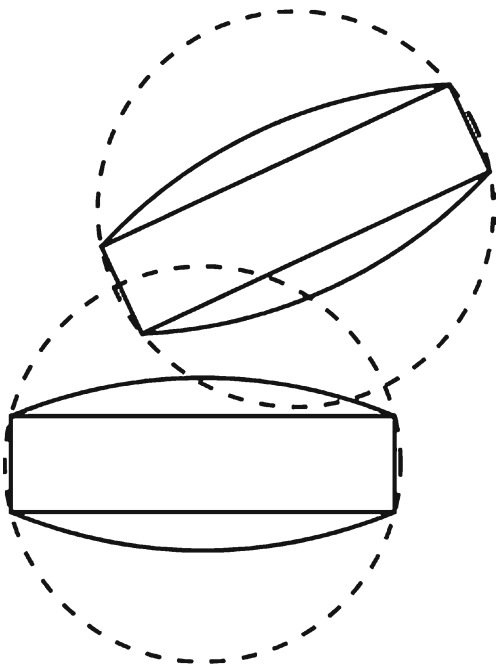

Fig. 3. Intermediate contact detection using the intersection of bounding spheres for two tablets. The contact scenario shown will not be filtered out since the bounding spheres intersect

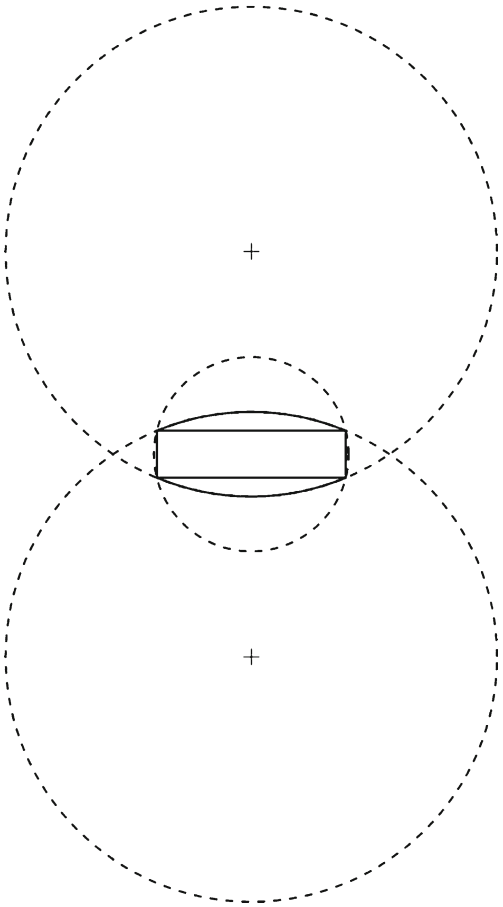

Fig. 4. Bounding sphere and the two cap spheres of a tablet. The centers of the cap spheres are indicated by *plus sign*

Contact Force Model

A contact force model takes the contact parameters determined by fine contact detection and computes the interaction force. In DEM, the forces are split into two components: a normal force, which acts along the normal direction at the point of contact, and a tangential force which acts in the direction of the relative tangential velocity. Stevens and Hrenya (21) review some of the normal contact force models commonly used in DEM and Di Renzo and Di Maio (22) discuss some tangential force models.

A viscoelastic damping model based on the assumption of a Hertzian quasi-static response and viscoelastic damping (23) is used for the current normal force model. This model was chosen due to the close agreement with the experimental data of contact duration and coefficient of restitution as a function impact velocity (21). For the tangential force, Coulomb's sliding friction model is used. Furthermore, similar to the single tablet model, the effects of atomizing and drying air on the motion of the tablets have been neglected.

Geometry

The diameter of the drum was selected to be 200 mm, which is a typical diameter for the O'Hara vibratory coater. The cylindrical drum geometry was approximated in the DEM simulations by a series of flat plates (similar to approximating a circle

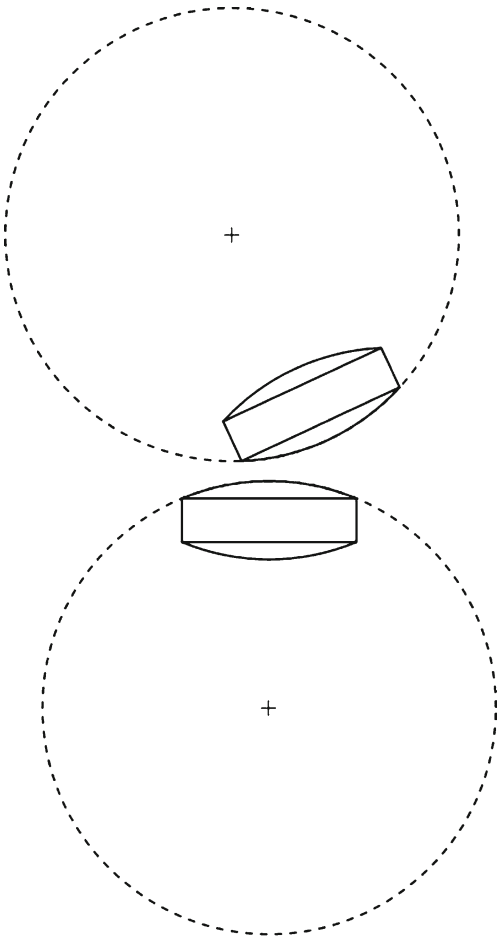

Fig. 5. Enhanced intermediate contact detection to filter out larger numbers of potential contacts. The contact scenario shown, which is the same as in Fig. 3, will be filtered out since the pair of spheres shown do not intersect

by a polygon) because algorithms for contact detection between a cylinder and a biconvex tablet have not been developed. A sensitivity study of the circulation speed was conducted with respect to the number of plates used to represent the cylindrical surface. The results indicate that the change in angular circulation speed (measured as discussed in the following section) was about 1% when the number of plates is changed from 96 to 128. Thus, for all the simulations, 96 plates were used along the full circumference of the drum to approximate the drum surface.

The length of the drum was 50 mm and the drum ends were set as periodic boundaries. The gap between the periodic

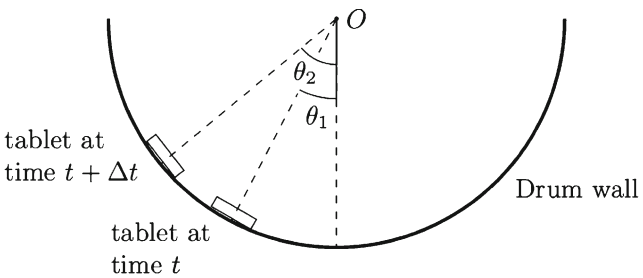

Fig. 6. Schematic showing the measurement of the angular circulation speed in the DEM simulations. Point O is the drum center. Angular circulation speed $\approx (\theta_2 - \theta_1)/\Delta t$

Table II. Parameters Used in the DEM Simulations

Parameter	Value
Tablet shape	Biconvex tablets (dimensions in Table I)
Tablet density	1,210 kg/m^3
Drum diameter	200 mm
Drum axial length	50 mm
Number of tablets	800
Normal contact force model	Viscoelastic Hertzian
Tangential contact force model	Coulomb sliding friction
Tablet Young's modulus	1×10^9 Pa
Drum Young's modulus	1×10^9 Pa
Tablet Poisson's ratio	0.3
Drum Poisson's ratio	0.3
Coefficient of sliding friction (tablet–tablet)	0.2
Coefficient of sliding friction (tablet–drum wall)	0.9
Coefficient of restitution (tablet–tablet)	0.575
Coefficient of restitution (tablet–drum wall)	0.8
Integration time step	2×10^{-6} s
Total simulation time	15 s

boundaries was chosen to be about five tablet diameters, which has been shown to be large enough so that the simulation results are not influenced by the distance between the periodic boundaries (24,25).

Angular Circulation Speed Measurements

The angular circulation speed of the tablets was measured by post-processing the tablet position data obtained from DEM simulations. Since the DEM simulations output absolute coordinates, the tablet position data is transformed to a frame of

Fig. 7. Snapshot from one of the DEM simulations

reference vibrating with the drum. The angular circulation speed, ω_{circ}, of a tablet can then be computed using,

$$\omega_{\text{circ}} = \frac{\theta(t+\Delta t) - \theta(t)}{\Delta t}, \tag{40}$$

where θ is the angle that the transformed position vector of the tablet makes with the vertical line passing through the drum center as shown in Fig. 6. Since the single tablet model predicts the motion of the tablets on the drum surface, the angular circulation speed measurements from DEM were also made only for tablets within one tablet diameter from the drum wall. The total number of measurements for each of the simulations ranged from 6,000 to 8,000.

DEM Simulation Setup

A summary of the parameters used in the DEM simulations is presented in Table II. Figure 7 shows a snapshot from one of the DEM simulations. Note that a closed drum is used in DEM simulations. However, whether the drum is open or closed at the top does not have any effect on the motion of the tablets since the tablets do not interact with that portion of the boundary.

The fill volume fraction, defined as the fraction of the drum volume occupied by the tablet bed, including the pores, was chosen to be 0.3, which is a typical value used in the pharmaceutical industry for tablet coating. A large value of 0.9 was chosen for the tablet–wall friction coefficient to prevent sliding of the tablets on the drum surface. The influence of friction coefficient is discussed further in the "Effect of Tablet–Wall Friction Coefficient". The tablet–tablet friction coefficient was measured using a pin-on-disk apparatus. For the coefficient of restitution between tablets and the drum wall, a value of 0.8 was used (26). A value of 0.575 was used for the coefficient of restitution between tablets (27).

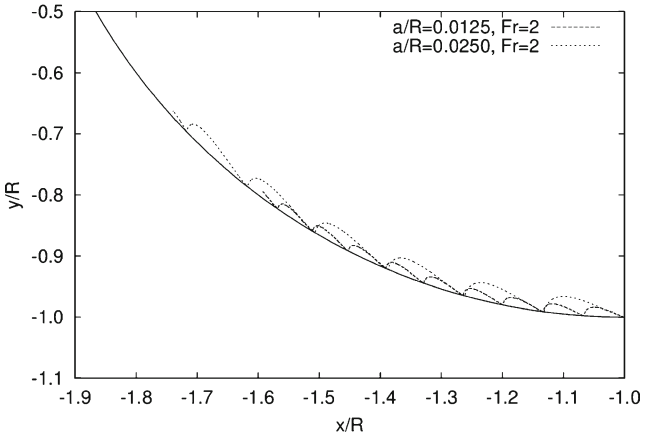

Fig. 9. Effect of a/R on the tablet trajectory as seen in the drum's frame of reference. The thick solid line represents the drum surface. Trajectories are shown until 0.5 s

RESULTS AND DISCUSSION

The equations of motion developed for the single tablet model suggest that a/R, Froude number, and the tablet–wall friction coefficient are significant parameters that influence the tablet trajectory and, hence, the angular circulation speed of tablets. The effect of each of these parameters on the angular circulation speed is presented in the following sections.

Effect of a/R and Froude Number

The effects of changing the dimensionless amplitude and the Froude number on the angular circulation speed of a tablet, ω_{circ}, are now considered. To simplify the algebra for analysis using the single tablet model, assume that the friction coefficient is large enough so that the tablet is never in the sliding phase. This case of "no sliding" represents the maximum angular circulation speed possible for a given a/R and

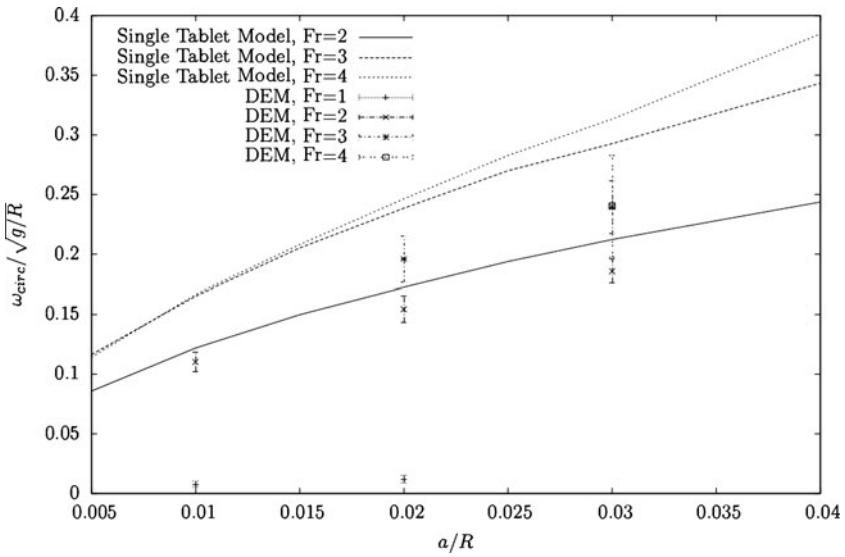

Fig. 8. Plot of angular circulation speed normalized by $\sqrt{g/R}$ as a function of a/R for different Froude numbers. For DEM simulations, a tablet–wall friction coefficient of 0.9 was used. Bars for DEM data indicate plus/minus one standard deviation of angular circulation speed. Note that the DEM data for a/R=0.03 and Fr=3 and 4 overlap

Froude number. For DEM simulations, a large value of the tablet–wall friction coefficient, equal to 0.9, was used between the tablet and drum walls to prevent the tablets from sliding on the drum surface.

Effect of *a*/*R*

First, the effect of changing the dimensionless amplitude ratio while keeping the Froude number constant is considered. The speed immediately after take-off is given by Eq. 30,

$$\left|\vec{v}\right| = 2a\omega\cos(\omega t)\cos\theta_0. \tag{30}$$

Thus, the speed is directly dependent on $\cos(\omega t)$, which does not change significantly if the Froude number is kept constant. However, $a\omega$ is expected to change significantly since it directly depends on the amplitude. Note that if the amplitude is changed, ω will also need to be adjusted in order to keep the Froude number constant. Using the definition of the Froude number,

$$\omega = \sqrt{Fr \cdot g/a}, \tag{41}$$

which leads to,

$$a\omega = \sqrt{Fr \cdot a \cdot g}. \tag{42}$$

Thus, the speed at which the tablet leaves the surface increases with increasing a/R implying that the tablet will travel a longer distance. Hence, the angular circulation speed of the tablets is also expected to increase with increasing a/R as shown in Fig. 8 for different values of Froude numbers, where the angular circulation speed has been normalized by $\sqrt{g/R}$. For a typical operation of the vibratory coater, the a/R is expected to be in the range of 0.02–0.04 while the Froude number is expected to be in the range of 2–5.

Figure 9 shows the trajectory of a tablet, solved numerically, for two different a/R but the same Froude number. The drum is initially in a horizontal position and the tablet is placed at the bottom-most point of the drum (θ_0=45 deg). The trajectory is computed using the equations of motion developed for the single tablet model until a final time of 0.5 s. The plot shows that the tablet travels farther along the drum for the larger a/R case and thus has a larger angular circulation speed.

The angular circulation speed measured from DEM simulations is also shown in Fig. 8. The angular circulation speed increases as a/R increases for a given Froude number. The predictions from the single tablet model over-predict the DEM results, but are reasonably close despite the simplicity of the model with the difference increasing at larger values of Froude number. Note that there is some scatter in the angular circulation speed values measured from DEM simulations due to the interaction between the tablets, which is not accounted for in the single tablet model.

Effect of Froude Number

Now examine the effect of changing the Froude number while keeping a/R constant. Note that Eq. 29 implies that for values of Froude number less than one the tablet will never leave the drum surface and thus the angular circulation speed will be zero (for the no-sliding case). However, if the exact condition in Eq. 28 is considered, rather than the approximation given by Eq. 29, the phase angle at which the tablet leaves the drum surface has a small dependence on a/R and the position of the tablet. Thus, the tablet may leave the drum surface at Froude numbers slightly smaller than one leading to a small angular circulation speed. DEM simulations were run at Froude number of one for different values of a/R. It can be seen from the values of angular circulation speed plotted in Fig. 8 that the angular circulation speed is close to zero, consistent with the single tablet model, which predicts no motion of the tablets for values of Froude number less than or equal to one.

As the Froude number increases, the speed at which the tablet leaves the surface also increases as shown by Eq. 42. However, due to the acceleration experienced by the tablet in the drum's frame of reference, the trajectory of the tablet becomes steeper with respect to the drum surface. Thus, initially the distance that the tablet travels, and hence the angular circulation speed, increases with increasing Froude number at smaller Froude numbers, but for larger values of the Froude number, the change in the angular circulation speed is not very large as shown by the tablet trajectories in Fig. 10. This effect

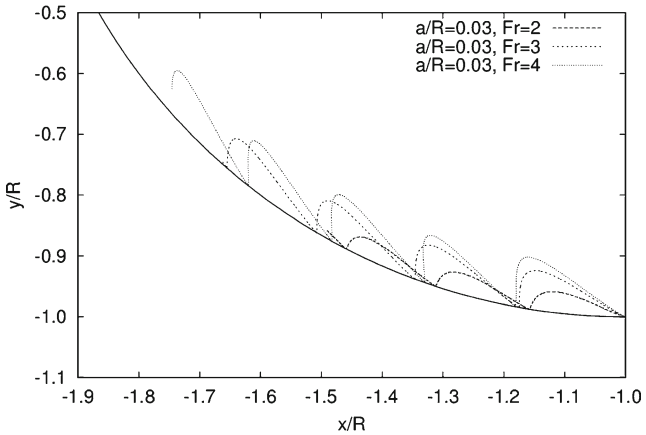

Fig. 10. Effect of Froude number on the tablet trajectory as seen in the drum's frame of reference. The thick solid line represents the drum surface. Trajectories are shown until 0.3 s

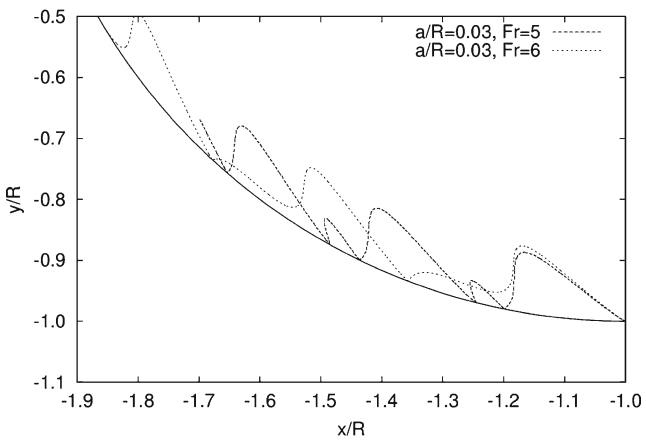

Fig. 11. Effect of large Froude numbers on the tablet trajectory as seen in the drum's frame of reference. The thick solid line represents the drum surface. Trajectories are shown until 0.3 s

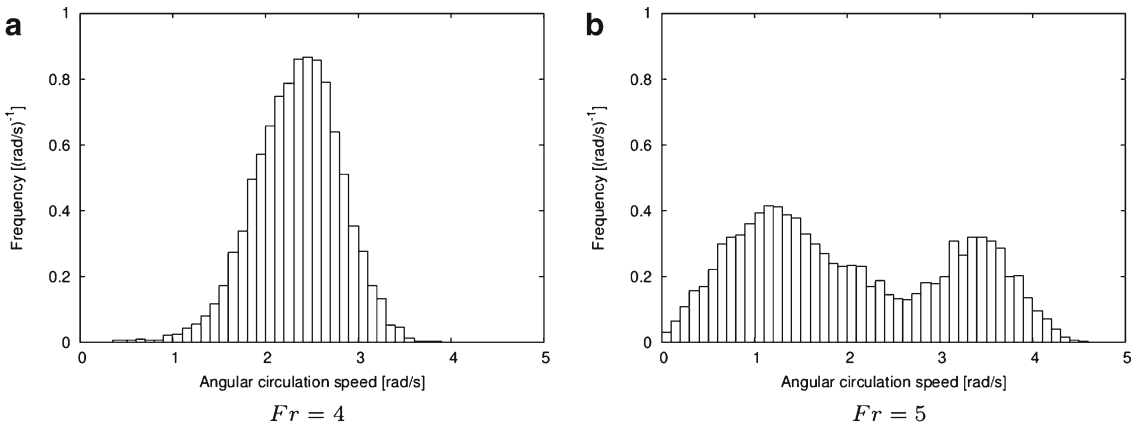

Fig. 12. Frequency distributions of angular circulation velocity for Froude numbers of four and five and a/R=0.03

of the Froude number on the angular circulation speed is also shown in Fig. 8 where for a given a/R, there is a significant increase in the angular circulation speed when the Froude number increases from two to three, but the change in angular circulation speed when the Froude number is further increased from three to four is not very large, due to the increasingly vertical trajectory of the tablet.

As the Froude number is further increased, new features start to appear in the tablet trajectory as shown in Fig. 11. At a Froude number of five, period-doubling is observed and the tablets hit the drum at two different phase angles while at a Froude number of six, the tablet impacts the drum once every two cycles instead of once every cycle. This phenomenon of period-doubling has also been reported by Wassgren *et al.* (18) for granular media subjected to vertical vibrations. Note that even though the single tablet model can predict the appearance of these phenomenon, the angular circulation speed predicted at these conditions by the model are not expected to be accurate since tablet–tablet interactions become strong at larger Froude numbers.

The results from the DEM simulations are plotted in Fig. 8. Similar to the single tablet model, the angular circulation speed increases as the Froude number increases from two to three. No change in the angular circulation speed was observed when the Froude number was increased from three to four. However, the scatter in the angular circulation speed increases at larger values of Froude number, which may be due to increased interaction between the tablets. This increased interaction at larger Froude numbers may also explain the difference in the angular circulation speed between the two models.

For larger values of Froude number, the tablets are expected to impact at different phase angles. Figure 12 shows the distribution of the angular circulation speed measured from DEM simulations for Froude numbers of four and five. Contrasting the two angular circulation speed distributions, two peaks are seen in the distribution for the larger Froude number. The tablet trajectory from the single tablet model suggests that this should indeed be the case. Due to the different phase angles at which the tablets impact the drum surface, two different trajectories are possible, one with a small angular circulation speed and another with a larger angular circulation speed (Fig. 11) leading to a large spread in angular circulation speed values. Note that from the point of view of tablet coating, this spread is not desirable since it may lead to a larger variance in the time the tablets spend in the spray and thus a larger coating variability.

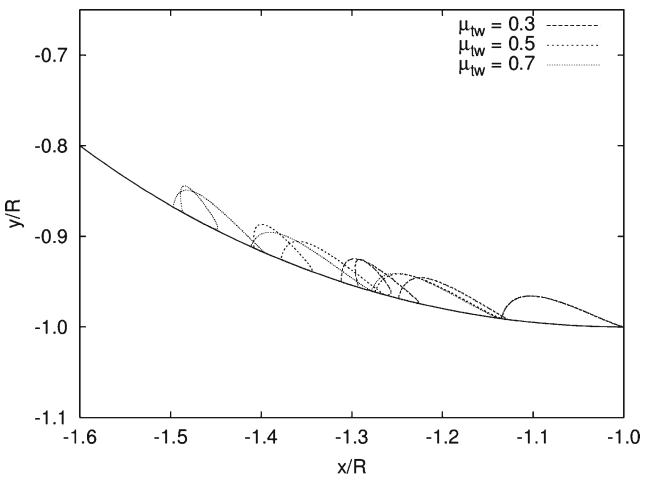

Fig. 13. Effect of tablet–wall friction coefficient on the tablet trajectory as seen in the drum's frame of reference. The *thick solid line* represents the drum surface

Effect of Tablet–Wall Friction Coefficient

Friction plays an important role in preventing the tablets from sliding back along the drum surface. If the tablet–wall

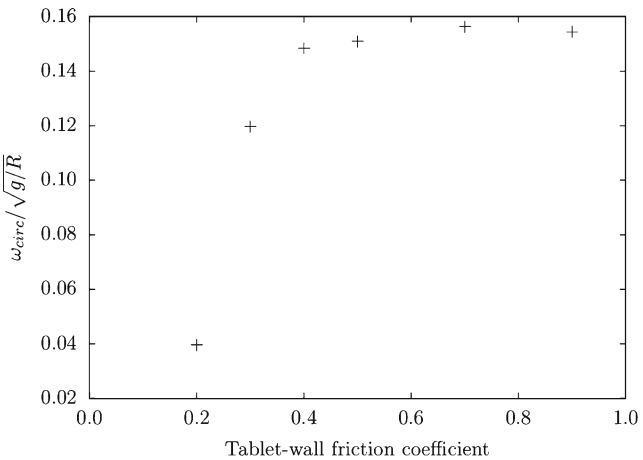

Fig. 14. Plot of angular circulation speed normalized by $\sqrt{g/R}$ as a function of the tablet–wall friction coefficient for Fr=2, a/R=0.02

friction coefficient is small, the friction force is also small, and tablets slide back down the drum surface reducing the angular circulation speed. Thus, the case of "no sliding" discussed in the previous section represents the maximum angular circulation speed possible for a given a/R and Froude number.

Figure 13 shows the tablet trajectory from the single tablet model for different values of the friction coefficient (but the same values of a/R and Froude number). As the friction coefficient increases, the tablet moves up higher along the drum before it starts to slide down. The angular circulation speed, however, could not be measured as a function of the friction coefficient since a well-defined trajectory of the tablet cannot be obtained due to the sliding of the tablets on the drum surface. Note that, in reality, a tablet is supported by the contact forces from other tablets, which prevents it from sliding down as much as the single tablet model predicts, even for smaller values of friction coefficient. This inability to account for contact forces between the tablets is one of the limitations of the single tablet model. Thus, this model cannot give accurate values for angular circulation speed when sliding is present and instead, a more detailed analysis such as the DEM model is required.

The effect of tablet–wall friction coefficient on the angular circulation speed of tablet was studied using the DEM simulations. Figure 14 plots angular circulation speed as a function of the tablet–wall friction coefficient while keeping the Froude number and a/R constant at 2 and 0.02, respectively. The angular circulation speed increases rapidly as the tablet–wall friction coefficient increases from 0.2 to 0.4 and then reaches an asymptote for larger values of friction coefficient. This trend in the angular circulation speed can be expected since the tablets slide back less for larger values of friction coefficient. Furthermore, when the friction coefficient is large enough to prevent the tablets from sliding back completely, the effect of the tablet–wall friction coefficient on the angular circulation speed is not very significant as shown by the small change in ω_{circ} for friction coefficients ranging between 0.4 and 0.9. Although, the tablet–wall friction coefficient is one of the difficult parameters to control, the DEM simulations suggest that larger friction coefficients provide better tablet circulation at least up to friction coefficients of 0.4. One of the ways in which the tablet–wall friction coefficient could be increased is to use (slightly) rougher walls for the drum.

CONCLUSIONS

The results from this study provide an understanding of how the vibration frequency and amplitude and the tablet–wall friction coefficient affect the circulatory motion of tablets in the coater. Larger angular circulation speed is preferred since it reduces the mean cycle time of tablets and tablets appear in the spray zone more frequently. Thus, a larger a/R, Froude number, and tablet–wall friction coefficient are recommended during the tablet coating operation. However, the Froude number should not be so large (>5) as to cause period doubling. Period doubling leads to an increase in the spread of the angular circulation speed and may adversely affect the coating uniformity. Note that the typical operating range of the vibratory coater is $a/R=0.02-0.04$ and Froude numbers 2–5, which are within the desirable operating range of these parameters. Although the tablet–wall friction coefficient is difficult to control, in practice, many coating drum are smooth and the tablet and coating formulations are such that the friction coefficient is small. Changing the pan surface to increase the effective friction coefficient, by modifying the texture or through the use of anti-slip bars, for example, would be beneficial from a coating variability perspective. Further work is on-going to validate these findings against experimental measurements of the angular circulation speed. Comparisons of predicted and measured inter-tablet coating mass variability are also desirable and will be made in a future study.

ACKNOWLEDGMENTS

The authors are grateful to the National Science Foundation Engineering Research Center for Structured Organic Particulate Systems (NSF ERC-SOPS, 0951845-EEC) for financial support. The authors would also like to thank Fritz Fiesser at Glaxo-Smith-Kline (GSK) for helpful suggestions.

REFERENCES

1. Thakral N, Thakral S. Continuous tablet coaters: developments, advantages and limitations. Innov Pharm Technol. 2009;70–3.
2. Marjeram J. Advantages of continuous pharmaceutical tablet coating. In: Tablets and capsules magazine. Saint Paul: CSC Publishing Inc. 2011.
3. Turton R. Challenges in the modeling and prediction of coating of coating pharmaceutical dosage. Powder Technol. 2008;181 (2):186–94.
4. Mann U. Analysis of spouted-bed coating and granulation. 1. Batch operation. Ind Eng Chem Process Des Dev. 1983;22 (2):288–93.
5. Denis C, Hemati M, Chulia D, Lanne JY, Buisson B, Daste G, *et al.* A model for surface renewal with application to the coating of pharmaceutical tablets in rotary drums. Powder Technol. 2003;130:174–80.
6. Freireich B. A compartmental approach to studying particle motion in mixer/coaters using discrete element modeling. Ph.D. thesis, Purdue University. 2010.
7. Kalbag A, Wassgren C. Inter-tablet coating variability: residence times in a horizontal pan coater. Chem Eng Sci. 2009;64:2705–17.
8. Suzzi D, Toschkoff G, Randl S, Machold D, Fraser S, Glasser B, *et al.* Dem simulation of continuous tablet coating: effects of tablet shape and fill level on inter-tablet coating variability. Chem Eng Sci. 2012;69:107–21.
9. Cunningham C, Hansell J, Nuneviller III F, Rajabi-Siahbhoomi AR. Evaluation of recent advances in continuous film coating processes. Drug Dev Ind Pharm. 2010;36(2):227–33.
10. Leaver T, Shannon H, Rowe R. A photometric analysis of tablet movement in a side-vented perforated drum (accela-cota). J Pharm Pharmacol. 1985;37:17–21.
11. Yamane K, Sato T, Tanaka T, Tsuji Y. Computer simulation of tablet motion in coating drum. Pharm Res. 1995;12:1264–8.
12. Sandadi S, Pandey P, Turton R. *In situ*, near real-time acquisition of particle motion in rotating pan coating equipment using imaging techniques. Chem Eng Sci. 2004;59: 5807–17.
13. Kalbag A, Wassgren C, Penumetcha S, Perez-Ramos J. Inter-tablet coating variability: residence times in a horizontal pan coater. Chem Eng Sci. 2008;63:2881–94.
14. Ng K, Ang L, Chng S. A computer model for vibrating conveyors. J Eng Manuf. 1986;200:123–30.
15. Lim G. Vibratory feeder motion study using turbo c++ language. Adv Eng Softw. 1993;18:53–9.

16. Lim G. On the conveying velocity of a vibratory feeder. Comput Struct. 1997;62(1):197–203.
17. Rademacher F, ter Borg L. On the theoretical and experimental conveying speed of granular bulk solids on vibratory conveyors. Eng Res. 1994;60(10):261–83.
18. Wassgren C, Brennan C, Hunt M. Vertical vibration of a deep bed of granular material in a container. Trans ASME. 1996;63:712–9.
19. Naeini S. Discrete element modeling of granular flows in vibrationally-fluidized beds. 2011. Ph.D. Thesis.
20. Kodam M, Curtis J, Hancock B, Wassgren C. Discrete element method modeling of bi-convex pharmaceutical tablets: contact detection algorithms and validation. Chem Eng Sci. 2012;69:587–601.
21. Stevens A, Hrenya C. Comparison of soft-sphere models to measurements of collision properties during normal impacts. Powder Technol. 2005;154:99–109.
22. Di Renzo A, Di Maio FP. Comparison of contact-force models for the simulation of collisions in DEM-based granular flow codes. Chem Eng Sci. 2004;59:525–41.
23. Kuwabara G, Kono K. Restitution coefficient in a collision between two spheres. Jpn J Appl Phys. 1987;26(8):1230–3.
24. Freireich B, Litster J, Wassgren C. Using the discrete element method to predict collision-scale behavior: a sensitivity analysis. Chem Eng Sci. 2009;64:3407–16.
25. Ketterhagen WR, Curtis JS, Wassgren CR. Stress results from two-dimensional granular shear flow simulations using various collision models. Phys Rev E. 2005;71:126–43.
26. Bharadwaj R, Smith C, Hancock B. The coefficient of restitution of some pharmaceutical tablets/compacts. Int J Pharm. 2010;402:50–6.
27. Antypov D, Elliott JA, Hancock BC. Effect of particle size on energy dissipation in viscoelastic granular collisions. Phys Rev E. 2011;84:021303.